RSC Advances

This is an *Accepted Manuscript*, which has been through the Royal Society of Chemistry peer review process and has been accepted for publication.

Accepted Manuscripts are published online shortly after acceptance, before technical editing, formatting and proof reading. Using this free service, authors can make their results available to the community, in citable form, before we publish the edited article. This *Accepted Manuscript* will be replaced by the edited, formatted and paginated article as soon as this is available.

You can find more information about *Accepted Manuscripts* in the Information for Authors.

Please note that technical editing may introduce minor changes to the text and/or graphics, which may alter content. The journal's standard Terms & Conditions and the Ethical guidelines still apply. In no event shall the Royal Society of Chemistry be held responsible for any errors or omissions in this *Accepted Manuscript* or any consequences arising from the use of any information it contains.

ROYAL SOCIETY OF CHEMISTRY

www.rsc.org/advances

Cite this: DOI: 10.1039/c0xx00000x

www.rsc.org/xxxxxx

COMMUNICATION

Fabrication of cuprous nanoparticles in MIL-101: An efficient adsorbent for the separation of olefin/paraffin mixtures

Ganggang Chang[†], Zongbi Bao[†], Qilong Ren[†], Shuguang Deng[†‡], Zhiguo Zhang[†], Baogen Su[†], Huabin Xing[†], and Yiwen Yang[†]*

Received (in XXX, XXX) Xth XXXXXXXXX 20XX, Accepted Xth XXXXXXXXX 20XX

DOI: 10.1039/b000000x

Various amounts of Cu^+ nanoparticles were successfully deposited to the pores of metal-organic frameworks MIL-101 with a double solvents method. An optimized cuprous loaded MIL-101 was shown to have an enhanced ethylene adsorption capacity and higher ethylene/ethane selectivity (14.0) compared to the pure MIL-101 (1.6). The great improvement of selectivity can be attributed to the newly generated nano-sized cuprous chloride particles that can selectively interact with the carbon-carbon double bond in ethylene through the π-complexation.

Separations of olefin/paraffin mixtures are one of the most energy-intensive processes in the chemical industry due to their very small relative volatilities and close molecular sizes.[1] Their separations performed at a large scale are currently achieved by cryogenic distillations, which are operated at low temperature (-30 °C) and high pressure (20 bar).[2] An alternative olefin/paraffin separation process with low energy consumption would significantly reduce operating expenses. Among all competing techniques toward this end, the adsorptive separation seems to be one of the most promising and energy-efficient processes.[2b] The adsorbent with adequate selectivity and capacity plays a crucial role in designing a practical adsorption process. To date, a number of solid adsorbents including zeolites,[3] activated carbon,[4] carbon molecular sieves,[5] and Ag(I) or Cu(I)-doped adsorbents,[6] have been evaluated for the adsorptive separation of olefin/paraffin mixtures. Recently, an emerging class of solid materials known as metal-organic frameworks (MOFs), which offer a high surface area, adjustable pore dimensions, and chemical tunability, have also been examined for olefin/paraffin separation.[7] In particular, MOFs with open metal sites like MOF-74 and HKUST-1, to some extent, show a potential in selective interactions with olefin by the π-complexation.[8] However, the MOFs with open metal sites also have a strong affinity toward water and are unstable when exposed to water vapor.[9] Besides, the ultra-microporous MOFs with their pore sizes close to the kinetic diameter of olefin, such as zeolitic imidazolate frameworks, show a remarkable kinetic effect in the separation of olefin from paraffin.[10]

Over the past decades, research efforts have been mostly aimed at preparing new MOF structures and studying their applications in molecule storage and separation.[11] Nowadays, loading of metal ions inside the porous matrices of MOFs is of current interest, and have been used as catalysts.[12] It has been reported that metal ions like Cu^+, Ag^+, Pd^{2+} and Pt^{2+} have a highly selective adsorption capability for compounds containing the C=C bond through a π-complex formation.[13] Among the numerous MOFs reported so far, MIL-101, synthesized by Ferey *et al.*,[14] is one of the excellent MOF materials due to its extra high specific surface area, pore volume, and high thermal and chemical stability to water as well as common organic solvents. The combination of these outstanding features makes it an interesting candidate for adsorption and catalysis. Moreover, the mesoporous cages can be used to confine the metal nanoparticles and to restrict their growth, which are the promising features for their applications in adsorption. However, to the best of our knowledge, no reports exist on the effect of Cu^+ nanoparticles in MOFs for ethylene and ethane separation. Herein, we reported the synthesis of a new π-complexation adsorbent by using MIL-101 as the support and cuprous chloride as the active component, of which CuCl was introduced to MIL-101 by the "double solvents" method.[12b] Furthermore, the Cu^+-supported MIL-101 (denoted as Cu^+@MIL-101) was evaluated for their adsorptive separation properties of ethylene and ethane to take advantage of the nano-sized Cu^+ sites for adsorption.

MIL-101, the highly crystallized green powder, was synthesized and purified according to the reported methods.[14,15] To avoid metal nanoparticles (NPs) aggregation on external surfaces of MIL-101 framework, we used the "double solvents" method for the synthesis of Cu^+@MIL-101.[12b] Scanning electron microscopy (SEM) images (Figure 1a) confirm that the synthesized MIL-101 is a highly crystallized regular octahedron with a perfect cubic symmetry. Transmission electron microscope (TEM) image (Figure 1d) confirms the cuprous loading and shows that the sizes of most Cu^+ nanoparticles are mainly in the range of 1.5-4.0 nm which are small enough to be accommodated in the mesoporous cavities of MIL-101.

Powder X-ray diffraction (PXRD) patterns shown in Figure 2 also confirm the structural integrity of the purified MIL-101. The main peaks of the MIL-101 match well with the PXRD pattern of the MIL-101 previously published by some investigators.[15,16] Figure 2(b, c) shows XRD patterns after Cu^+ loaded. Clearly, when the loading amount is less than 50wt%, Cu^+ can get good dispersion on MIL-101 and the dispersion is under the monolayer

RSC Advances Accepted Manuscript

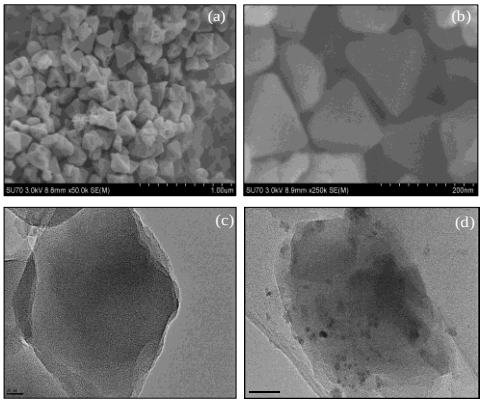

Figure 1. SEM images of (a, b) MIL-101 and TEM images of (c) MIL-101, (d) 40wt%Cu^+@MIL-101.

dispersion amount.[17] However, when the loading amount exceeds 50wt%, three major diffraction peaks at 28.5°, 47.5°, and 56.3° are observed. These peaks can be assigned to CuCl indicating the aggregation of Cu^+ on the surface of MIL-101. Besides, the main peaks of the MIL-101 are still remained, demonstrating the remained intact structure of MIL-101 after Cu^+ loaded.

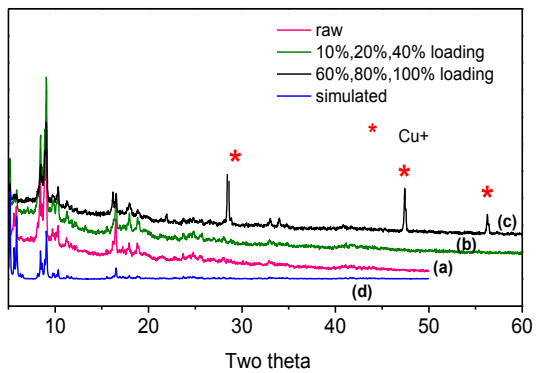

Figure 2. X-ray patterns for Cu^+-loaded MIL-101 samples with different CuCl loadings. (a) raw ; (b)10%, 20%, 40wt% loading; (c) 60%, 80%, 100wt% loading; (d) simulated.

To further confirm the cuprous loading, X-ray photoelectron spectroscopy (XPS) were also performed. The presence of Cu^+ is supported by the XPS spectrum that is similar to that of CuCl rather than $CuCl_2$ (Figure 3). In addition, the BET surface area and pore volume of the Cu^+@MIL-101 are analysed and summarized in Table S1. For Cu^+@MIL-101 with 40wt% loading, the BET surface area significantly decreases from 3120 to 1587 m^2/g and the pore volume also decreases from 2.12 to 1.01 cm^3/g after loading the CuCl, which confirms that the Cu^+ nanoparticles are successfully dispersed within the pores of MIL-101. Also the sacrificed cumulative volume contributed by mesopores around 2.5 nm can be observed from the pore size distribution curve shown in Figure S1.

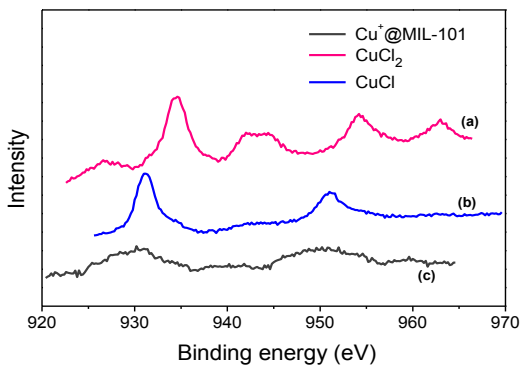

Figure 3. XPS spectra of Cu regions of Cu^+@MIL-101. (a) $CuCl_2$; (b) CuCl; (c) 40%wtCu^+@MIL-101.

Single-component adsorption isotherms of ethylene and ethane at 303 K and 1 bar on the pure and composite MIL-101 adsorbents loaded with different Cu^+ amounts are shown in Figure S4, and all the adsorption isotherms could be well described by the double-site Langmuir model. The Henry constant (H), equilibrium selectivity (α), and adsorbent selection parameter (S) are summarized in Table S1. The introduction of Cu^+ leads to a preference for C_2H_4 adsorption at 1 bar (from 2.2 to 2.75 mmol/g) and an obviously enhanced selectivity of ethylene over ethane (from 1.6 to 16.5), and the selectivity increases with the loading of Cu^+. Figure 4 compares the isotherms on the undoped MIL-101, 40wt%Cu^+@MIL-101 and pure CuCl. Interestingly, the pure CuCl almost shows no ethylene adsorption due to its negligible specific surface area. Therefore, for enhancing ethylene adsorption, well dispersed and nano-sized particles of Cu^+, which offer larger surface areas, are really important. The enhanced C_2H_4 uptake and selectivity can be ascribed to the well-dispersed Cu^+ that generates additional adsorption active sites on MIL-101 and increases the energetic heterogeneity of the surface, while these newly generated Cu^+ sites can selectively interact with the C=C bond in ethylene through a π-complexation. Meanwhile, the original physical adsorption sites on MIL-101 are covered by Cu^+, which leads to the decrease of ethane uptake. Furthermore, the more Cu^+ ions are introduced, the less physical adsorption sites remain. As a result, the Cu^+ loaded MIL-101 samples exhibit a selective adsorption of ethylene over ethane. However, when Cu^+ loading is relatively high (>50wt%), some pores were blocked by the larger aggregates formed from the growth of smaller Cu^+ nanoparticles, thus decreased the ethylene uptake.

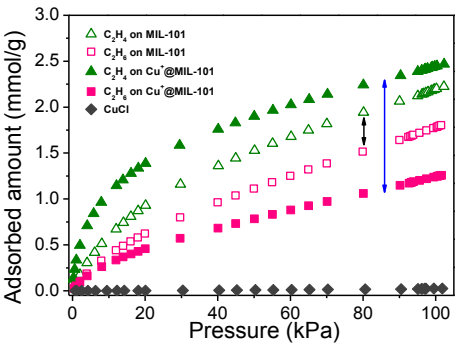

Figure 4. Ethylene and ethane isotherms for the pure, 40wt%Cu^+ loaded MIL-101 and pure CuCl at 30°C and 1bar.

Additionally, the Ideal Adsorbed Solution Theory (IAST) [18] was applied to predict the selectivity for separating a mixture of ethylene and ethane. The selectivity of C_2H_4/C_2H_6 with different molar fractions and varied total pressures are shown in Figure S6. The C_2H_4/C_2H_6 selectivity of 40wt% Cu^+-loaded MIL-101 is much higher than that of the undoped MIL-101, despite different molar fractions of the two adsorbates. For an example, the

RSC Advances Accepted Manuscript

This journal is © The Royal Society of Chemistry [year]

C_2H_4/C_2H_6 selectivity is 1.76 on the undoped MIL-101 at a C_2H_4 molar fraction of 0.2 while a selectivity of 8.7 is obtained on Cu^+-loaded MIL-101. The selectivity with total pressures ranging from 1 to 4 bar were also calculated, of which the composition was fixed at 50:50% and reaffirmed that C_2H_4/C_2H_6 selectivity could be largely enhanced by loading Cu^+. We summarized the most widely used adsorbents for C_2H_4/C_2H_6, their equilibrium uptake at about 30°C and 1bar are listed in Table S2. Obviously, the traditional adsorbents like activated carbon and zeolites have a low uptake capacity although some have a high selectivity up to 2.52. In contrast, metal-organic frameworks with open metal sites usually have a high adsorption amount but the poor selectivity is impractical for an industrial adsorption process.

To further investigate the affinity after modification of MIL-101, single-component gas adsorption isotherms (Figure S5) were measured on Cu^+@MIL-101 with 40wt% loadings of CuCl at 1 bar and temperatures varied from 303K to 323K. The initial isosteric heats (Figure S7) for ethylene and ethane are found to be about 40 and 25 kJ/mol, respectively. These moderate values are comparable with that on 13X zeolite, [3b] $Cu_3(BTC)_2$ [8b] and Mg-MOF-74 [8c]. The kinetic adsorption profiles of ethane, ethylene recorded at pressure of 60 mmHg and 298 K are shown in Figure S8. There is no significant reduction in diffusion kinetics for ethane/ethylene adsorption after the Cu^+ nanoparticles confined in the cages. The intracrystalline diffusivity D_c/r_c^2 for ethane and ethylene in the undoped and 40wt% Cu^+@MIL-101 studied in this work were 5.72×10^{-2}, 2.85×10^{-2}, 3.79×10^{-2}, 2.06×10^{-2} s^{-1}, respectively. The decreased diffusion time constants for ethane-ethylene pair in the Cu^+@MIL-101 also double check the successful deposition of Cu^+ NPs. The slower kinetics were observed in ethylene compared to ethane in both undoped and Cu^+@MIL-101, which can be explained by the enhanced surface interaction energy between Cu^+ and ethylene by the π-complexation.[19]

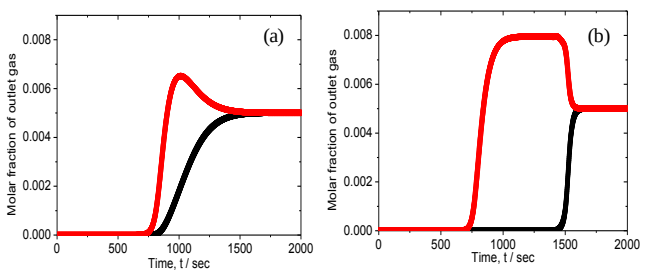

Figure 5. Breakthrough curves of equimolar mixtures of ethane/ethylene in columns of MIL-101(a) and Cu^+@MIL-101 (b) at 303.15 K and 1 bar calculated using Aspen™.(black: ethylene, red: ethane)

To compare the adsorptive separation between raw MIL-101 and Cu^+-doped MIL-101, we performed transient packed bed breakthrough calculations using Aspen™ Adsorption module. Figure 5 provide a comparison of the breakthrough characteristics for 50/50 ethane/ethylene mixture at 303.15 K and 1 bar, for the MIL-101 and Cu^+-doped MIL-101. It was obviously observed that the ethylene adsorption capacity was significantly improved in case of Cu^+-doped MIL-101. In summary, we demonstrated the successful deposition of Cu^+ nanoparticles in porous MIL-101 through a double solvents method. A well-dispersed Cu^+ loaded MOF maintained its structure, and exhibited higher C_2H_4 uptake and higher ethylene/ethane selectivity (14.0) compared to the undoped MIL-101 (1.6). This can be attributed to the newly generated Cu^+ sites that can selectively interact with the C=C bond in ethylene through the π-complexation.

This work was supported by the National Natural Science Foundation of China (21376205 and 20936005), the Zhejiang Provincial Natural Science Foundation of China (LR13B060002), and the Zhejiang Province Key Science and Technology Innovation Team (2011R50002).

Notes and references

Key Laboratory of Biomass Chemical Engineering of Ministry of Education, Department of Chemical and Biological Engineering, Zhejiang University, Hangzhou 310027, China. E-mail: baozb@zju.edu.cn; Fax:86-571-87952773; Tel: 86-571-87952773

† Electronic Supplementary Information (ESI) available: Details of synthesis, adsorption experiments and characterization are included. See DOI: 10.1039/b000000x/

1 T. Ren, M. Patel and K. Blok, *Energy*, 2006, **31**, 425-451.
2 a) D. M. Ruthven and S. C. Reyes, *Micropor. Mesopor. Mater.*, 2007, **104**, 59-66; b) N. Lamia, M. Jorge, M. A. Granato, F. A. Almeida Paz, H. Chevreau and A. E. Rodrigues, *Chem. Eng. Sci.*, 2009, **64**, 3246-3259.
3 a) F. A. Da Silva and A. E. Rodrigues, *Ind. Eng. Chem. Res.*, 1999, **38**, 2051-2057; b) C. A. Grande, J. Gascon, F. Kapteijn and A. E. Rodrigues, *Chem. Eng. J.*, 2010, **160**, 207-214.
4 B.-U. Choi, D.-K. Choi, Y.-W. Lee and B.-K. Lee, J. Chem. Eng. Data, 2003, 48, 603-607.
5 a) T. Nakahara and T. Wakal, *J. Chem. Eng. Data*, 1987, **32**, 114-117; b) C. A. Grande and A. E. Rodrigues, *Ind. Eng. Chem. Res.*, 2004, **43**, 8057-8065.
6 a) F. J. Blas, L. F. Vega and K. E. Gubbins, *Fluid Phase Equilib.*, 1998, **150-151**, 117-124; b) F. Iucolano, P. Aprea, D. Caputo, C. Colella, M. Eić and Q. Huang, *Adsorption*, 2008, **14**, 241-246.
7 a) Y. B. He, S. C. Xiang, Z. J. Zhang, S. S. Xiong, F. R. Fronczek, R. Krishna, M. O' Keeffe and B. L. Chen, *Chem.Commun.*, 2012, **48**, 10856-10858; b) Y. B. He, R. Krishna and B. L. Chen, *Energy Environ. Sci.*, 2012, **5**, 9107-9120.
8 a) E.D. Bloch, W.L. Queen, R. Krishna, J.M. Zadrozny, C.M. Brown and J.R. Long, *Science*, 2012, **335**, 1606-1610; b) S. Wang, Q. Yang and C. Zhong, *Sep. Purif. Technol.*, 2008, **60**, 30-35; c) Z. Bao, S. Alnemrat, L. Yu, I. Vasiliev, Q. Ren, X. Lu and S. Deng, *Langmuir*, 2011, **27**, 13554-13562.
9 a) A. C. Kizzie, A. G. Wong-Foy and A. J. Matzger, *Langmuir*, 2011, **27**, 6368-6373; b) P. M. Schoenecker, C. G. Carson, H. Jasuja, C. J. J. Flemming and K. S. Walton, *Ind. Eng. Chem. Res.*, 2012, **51**, 6513-6519;c) Y. Cai, Y. Zhang, Y. Huang, S. R. Marder and K. S. Walton, *Cryst. Growth Des.*, 2012, **12**, 3709-3713.
10 a) C. Gucuyener, J. v. d. Bergh, J. Gascon and F. Kapteijn, *J. Am. Chem. Soc.*, 2010, **132**, 17704-17706; b) K. Li, D. H. Olson, J. Seidel, T. J. Emge, H. Gong and H. Zeng, *J. Am. Chem. Soc.*, 2009, **131**, 10368-10369.
11 a) J.-R. Li, J. Sculley and H.-C. Zhou, *Chem. Rev.*, 2012, **112**, 869-932; b) J.-R. Li, R. J. Kuppler and H.-C. Zhou, *Chem. Soc. Rev.*, 2009, **38**, 1477 .
12 a) N. Maksimchuk, M. Timofeeva, M. Melgunov, A. Shmakov, Y. Chesalov, D. Dybtsev, V. Fedin and O. Kholdeeva, *J.Catal.*, 2008, **257**, 315; b) A. Aijaz, A. Karkamkar, Y. J. Choi, N. Tsumori, E. Rönnebro, T. Autrey, H. Shioyama and Q. Xu, *J. Am. Chem. Soc.*, 2012, **134**, 13926-13929; c) M. A. Gotthardt, A. Beilmann, R. Schoch, J. Engelke and W. Kleist, *RSC Adv.*, 2013, **3**, 10676-10679
13 a) N. A. Khan and S. H. Jhung, *J. Hazard. Mater.*, 2012, **237-238**, 180-185; b) W.-J. Jiang, Y. Yin, X.-Q. Liu, X.-Q. Yin, Y.-Q. Shi and L.-B. Sun, *J. Am. Chem. Soc.*, 2013, **135**, 8137-8140; c) N. A. Khan and S. H. Jhung, *Angew. Chem. Int. Ed.*, 2012, **51**, 1198-1201; d) W. P. Qin, W. X. Cao, H. L. Liu, Z. Li and Y. W. Li, *RSC Adv.*, 2014, **4**,2414-2420.

RSC Advances Accepted Manuscript

14 G. Ferey, C. Mellot-Draznieks, C. Serre, F. Millange, J. Dutour, S. Surble and I. Margiolaki, *Science*, 2005, **309**, 2040-2042.
15 K. Yang, Q. Sun, F. Xue and D. Lin, *J. Hazard. Mater.*, 2011, **195**, 124-131.
16 Z. Zhao, X. Li and Z. Li, *Chem. Eng. J.*, 2011, **173**, 150-157.
17 Y.C. Xie and Y.Q. Tang, *Adv. Cata.*, 1990, **37**, 1.
18 Z. J. zhang, Z. Li and J. Li, *Langmuir*, 2012, **28**, 12122-12138.
19 R. Krishna and J. M. Van Baten, *Phys. Chem. Chem.Phys.*, 2013, **15**, 7994-8016.

RSC Advances Accepted Manuscript

This journal is © The Royal Society of Chemistry [year]